8th European Workshop On Structural Health Monitoring (EWSHM 2016), 5-8 July 2016, Spain, Bilbao
www.ndt.net/app.EWSHM2016

Numerical Characterization of Mechanochromic Photonic Crystals for Structural Health Monitoring

Valentina PICCOLO [1,2], Anna PIOTROWSKA [3], Andrea CHIAPPINI [3], Alessandro VACCARI [4], Maurizio FERRARI [3], Luca DESERI [2,6,7,8], Daniele ZONTA [1,3,5]

[1] University of Trento, Via Mesiano 77, 38123, Trento, Italy
[2] MEMS-Swanson School of Engineering, University of Pittsburgh Benedum Hall, 3700 O'Hara Street, Pittsburgh, PA 15261 USA
[3] Institute for Photonics and Nanotechnologies, National Research Council, Via alla Cascata 56/C, 38123 Trento, Italy
[4] Fondazione Bruno Kessler, Via Sommarive, 18, 38123, Trento, Italy
[5] University of Strathclyde Glasgow, 16 Richmond St, Glasgow G1 1XQ, Regno Unito
[6] MACE-Div. Aerospace Engineering, College of Engineering, Design and Physical Sciences, Brunel University London, Uxbridge, UB8 3PH, United Kingdom
[7] Dept. of Mech.Eng Dept. Carnegie Mellon University, Pittsburgh PA 15213-3890 USA
[8] Department of Nanomedicine, The Methodist Hospital Research Institute, 6565 Fannin St., MS B-490 Houston, TX 77030 USA

Abstract

We discuss the possible use of photonic crystals as strain sensors. We demonstrate the feasible fabrication of a crystal having sub-micrometric polystyrene colloidal spheres in a PDMS matrix on a rubber substrate, and we demonstrate that the photonic properties change *with substrate elongation according to theoretical prediction. The crystal's sensitivity to* strain depends di*rectly on interplanar spacing and on Poisson's ratio. To enhance the crystal* strain resolution, we propose to fabricate inverse photonic structures, which exhibit a high geometrical Poisson's ratio, and we investigate their photomechanical behavior through non-linear Finite Element analysis.

Keywords: Smart structures, Modeling, Experimental validation, Industrial applications

1. INTRODUCTION

A photonic crystal (PhC) is a periodic structure with periodicity comparable with the wavelength of light, having a photonic band gap in the visible range. A photonic structure reflects a band of the incident light, so it appears to an observer to be of a certain color. Photonic crystals occur in nature [1] and can be artificially produced [2,3,4]. Synthetic opals are an example of artificial photonic crystals produced by vertical deposition. They are made using colloidal spheres in solution, organized as a 3-dimensional crystalline lattice. The size of the spheres and their polydispersivity are such that the crystal acts as a periodic photonic band gap or as a narrow-band mirror. These structures can be used in photonic devices such as switches, mirrors, filters and superprisms [5]. This kind of PhC can be fabricated as a soft film deposited on a flexible support. Spheres can be of silica or polystyrene, with diameters varying from 100 to 1000nm, and the opal PhC can be infiltrated with several solution types, for example an elastomer.
The idea of using the crystal as a sensor is based on the observation that distortion in the crystal structure changes the reflected bandwidth. Fiber Bragg Gratings (FBGs) are a well-

known example of a photonic structure commonly used as sensors in civil and mechanical applications [6,7,8,9,10,11], although they normally operate in the infrared field. When a photonic crystal is designed to operate in the visible spectrum, a permanent distortion of the crystal lattice results in a change in its apparent color. Fudouzi [12,13] has suggested that these crystals can also be used in optical strain sensors, suitable for monitoring and displaying structural and environmental variation in terms of color change, seen by both by appropriate optical instruments or by the naked eye. This property makes photonic crystals suitable for permanent monitoring of structural elements, as any critical change in the strain field can be seen promptly and easily.

Some limits of this technology have been highlighted in [14]. In this contribution we discuss how we can overcome these limits by exploiting the mechanical properties of inverse photonic crystals, which are 3D structures where the solid colloidal spheres are replaced by voids. They are normally produced from a direct colloidal sphere 3D opal, by dissolving the spheres with a solvent [15]. In the next section we introduce the basic formulation that controls the photo-mechanical behavior of a 3D photonic crystal. We describe the production process for a direct opal and we demonstrate its photonic properties in a laboratory experiment.

2. APPROXIMATE OPTOMECHANCAL APPROACH

Consider the 3D photonic crystal schematically depicted in Fig.1a, made of colloidal spheres into an elastomeric matrix of refractive indices n_1 and n_2, respectively, and filling factor f. Illuminated by white light with zero incidence angle, the crystal reflects light around a specific band-gap wavelength λ. As a first approximation this is expressed by Bragg's law [16]:

$$\lambda = 2 \cdot n_{eff} \cdot d \qquad (1)$$

where d is interplanar distance and n_{eff} is the effective refractive index of the crystal determined as follows:

$$n_{eff}^2 = f \cdot n_1^2 + (1 - f) n_2^2 \qquad (2)$$

Thus, a "small" change in the interplanar spacing d will result in a change in reflected wavelength according to:

$$\Delta\lambda = 2 \cdot n_{eff} \cdot \Delta d = 2 \cdot n_{eff} \cdot d_0 \cdot \varepsilon_3 \qquad (3)$$

where ε_3 is the crystal (small) strain in the direction orthogonal to its plane and d_0 is the interplanar spacing in unstrained condition. This method applies in the context of infinitesimal strain. The crystal is adherent to a substrate and it is subject to a plain stress condition. Obviously the vertical contraction is related to the two in-plane strain components of the substrate through the following relationship:

$$\varepsilon_3 = -\frac{\nu}{1-\nu}\{\varepsilon_1 + \varepsilon_2\} \qquad (4)$$

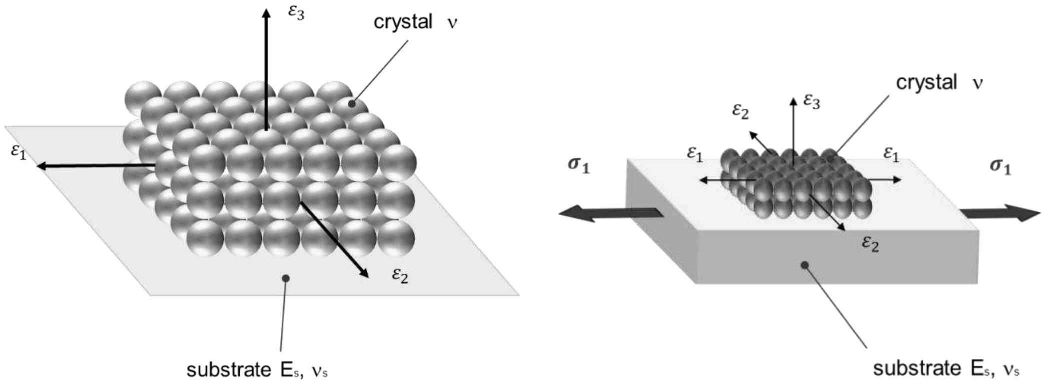

a) b)

Figure 1. (a) Three dimensional photonic crystal on the substrate without stress application; b) the same configuration with stress applied (σ_1) and related to them strain distribution (ε_1, ε_2, ε_3); E_s, ν_s are Young modulus and Poisson's ratio for substrate, ν Poisson's ratio for photonic crystal.

If we apply a stress σ_1 to the substrate in direction 1, this will result in an elongation ε_1 in the same direction and in two contractions in the two orthogonal directions. The one in the same plane of the substrate, ε_2, can be evaluated with the following formula:

$$\varepsilon_2 = -\nu_s \varepsilon_1, \tag{5}$$

where ν_s is and Poisson's coefficient of the substrate. Replacing (5) in (4), we obtain:

$$\varepsilon_3 = -\nu \frac{1-\nu_s}{1-\nu} \varepsilon_1 \approx -\nu \varepsilon_1 \tag{6}$$

where the approximation is valid as long as as the two Poisson's rations are close enough. Equation 6 basically states that when the substrate is stretched under a uniaxial stress in one in-plane direction, the crystal contracts approximately ν times the elongation along the stress direction. Combining (6) with (3) we finally determine the following expression for change in reflected wavelength $\Delta\lambda$:

$$\Delta\lambda \approx -2 \cdot \mathrm{n_{eff}} \cdot \nu \cdot \mathrm{d}_0 \cdot \varepsilon_1 \tag{7}$$

In the most general case both the refractive index n_{eff} and Poisson's ratio ν could change with strain. Henceforth, the relationship between the bandgap wavelength and the transverse strain becomes nonlinear. In this case the sensitivity of $\Delta\lambda$ with the change in longitudinal strain takes approximately the following form:

$$\frac{\mathrm{d}\lambda}{\mathrm{d}\varepsilon_1} \approx -2 \cdot \mathrm{d}_0 \cdot \left\{ \frac{\mathrm{dn_{eff}}}{\mathrm{d}\varepsilon_1} \cdot \nu \cdot \varepsilon_1 + \mathrm{n_{eff}} \cdot \frac{\mathrm{d}\varepsilon_3}{\mathrm{d}\varepsilon_1} \right\}. \tag{8}$$

By assuming a linearly elastic behavior of the material and the effective refraction index n_{eff} constant with strain, equation (8) reduces to the following expression:

$$\frac{\mathrm{d}\lambda}{\mathrm{d}\varepsilon_1} \approx -2 \cdot \mathrm{n_{eff}} \cdot \nu \cdot \mathrm{d}_0, \tag{9}$$

which basically shows that the crystal sensitivity to strain is proportional to its refractive index, lattice spacing and Poisson's ratio.

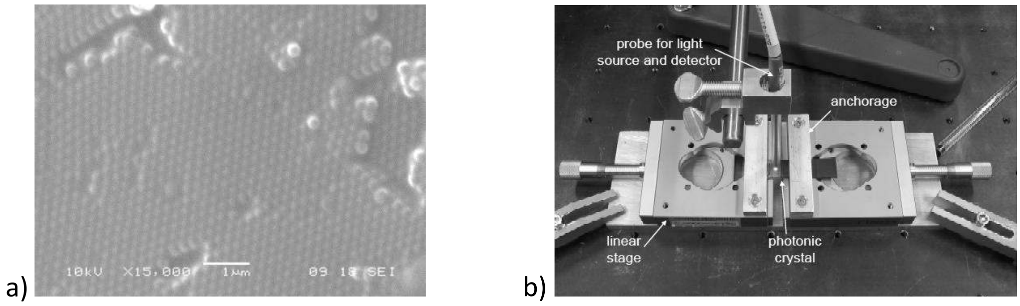

Figure 2. (a) Scanning Electron Microscopy (SEM) picture of the crystal and (b) test setup [10].

3. MATERIALS AND METHODS

A prototype of colloidal PhC was fabricated and tested in the laboratory. The crystal, of dimensions 10×10 mm, was manufactured through deposition over a 50×15×1 mm rubber substrate of 230 nm polystyrene spheres, infiltrated with poly-dimethylsiloxane (PDMS). Details of the fabrication process are reported in [17]. Figure 2a shows a Scanning Electron Microscopy (SEM) image of the PhC: the interplanar spacing is 280 nm, resulting in a bandgap wavelength of 582 nm.

During the test, the substrate strip was fastened to two micrometric linear stages, as shown in Figure 2b, and stretched in uniaxial condition to different strain levels. At each step, the reflectance of the PhC in the visible range using a spectrometer was recorded with a wavelength resolution of 0.1nm. Figure 3a shows the reflectance obtained for different values of the longitudinal strain, while Fig.3b plots the experimental relationship between reflectance peak wavelength and strain, as recorded during the test. As predicted by Equation (9), the wavelength decreases with strain and, below 120 mε, the relationship is approximately linear. In particular, the experimental sensitivity to strain and its inverse are:

$$\frac{\mathrm{d}\lambda}{\mathrm{d}\varepsilon} = \text{-0.288 pm/}\mu\varepsilon \ ; \ \frac{\mathrm{d}\varepsilon}{\mathrm{d}\lambda} = \text{-3.47 }\mu\varepsilon\text{ /pm} \qquad (10)$$

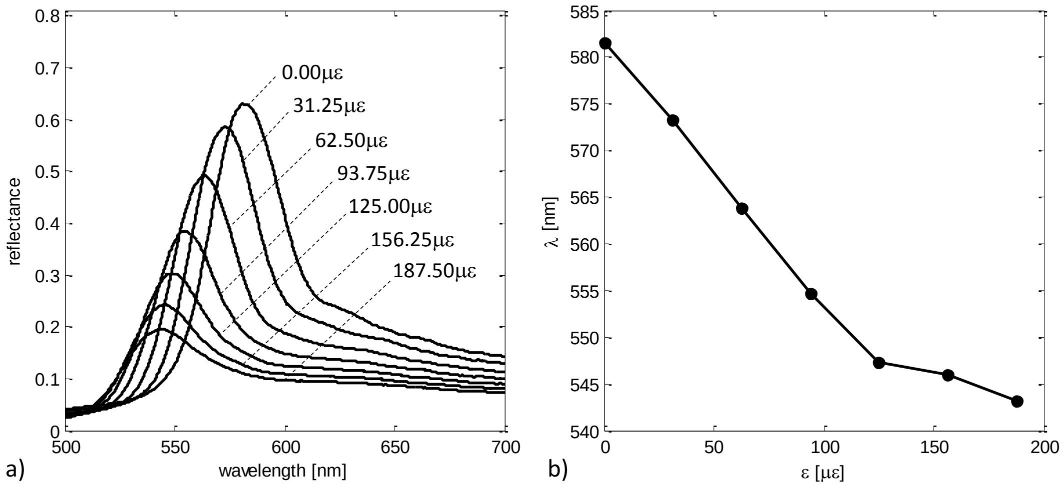

Figure 3. Reflectance spectra (a) of the colloidal PhC recorded during the elongation test and (b) experimental relationship between bandgap wavelength and strain.

If the maximum reflectance peak can be resolved with an accuracy of 0.1 nm, this corresponds to instrumental resolution of about 350 με. Such a resolution is acceptable for applications where the strain to be measured is a few percent. The latter circumstance though would invalidate the assumption of geometric linearity, namely infinitesimal strains, and also the material response would be nonlinearly elastic. Nonetheless such accuracy is actually not sufficient for civil and mechanical engineering applications, where often times the materials involved in the monitoring are steel and concrete, and so where a strain resolution the order of 5 με is typically required.

Equation (9) suggests that the resolution is easily improved by increasing the crystal interplanar spacing, for example by changing the size of the beads and/or by multiplying the swelling/infiltration cycles. However this will result in a crystal which does not work in the visible range. Such a devise has then to be interrogated exclusively with instrumentation, thereby losing the feature that makes it appealing for monitoring applications. The same Equation (9) also shows that the sensitivity is proportional to the Poisson's ratio ν; this means that the resolution of the device could be improved by choosing either a material or a microstructural configuration with a higher magnitude Poisson's ratio than the usual materials. This possibility is explored in the next section.

4. PHOTONIC CRYSTAL SLABS, A NOVEL CONCEPT

A new application for photonic crystal slabs is here envisioned. As discussed above, 3D photonic crystals are technologically challenging structures and their accuracy is not yet the one required for civil applications. A good compromise in terms of structure simplicity and light manipulation in all spatial directions are the photonic crystal slabs (PCSs) [18]. This kind of crystals consists of a dielectric layer exhibiting a periodic structure with a higher refractive index relative to its environment. From a manufacturing point of view, the PCSs can either be free standing slabs in air (air-bridge) or be realized on a substrate; the latter is mechanically more stable. In this manuscript, we explore the quadratic and the hexagonal structure of the PCSs. These two types of structures are more interesting because they show a periodicity in both x and y space direction. There are two effects that cause light manipulation in all spatial directions: the first (manipulation of light in the plane) is the periodicity of the structure with very different refractive indexes, which in our case are the material forming the layer and the air in holes in the layer itself; the second is that the light perpendicular to the plane is restricted locally partly by total internal reflection and partly by simple reflection.

Negative Poisson's effects can be envisaged for such structures, as suggested by experiments at a much larger scales and in the case of plane stress [15, 16]. Nonetheless, among natural and artificial materials many of them are characterized by a positive Poisson's ratio. The values range from zero (as in the case of cork) to 0.5 (as in the case of some rubbers), but most commonly of the order of 0.2 ÷ 0.3 (e.g. 0.3 for steel and PDMS). Well known thermodynamic restrictions in isotropic linear elasticity owe the Poisson's ratio in the interval -1, 0.5 and it is clear that in the linear regime such a ratio is a intrinsic material property. Of course if the strain regime is nonlinear, namely with values of principal strains higher than 10^{-3}, then the Poisson's ration loses the feature of being a genuine property of the material. Because of this, local versus global strain dependent Poisson's ratios must also be investigated. Although highly desirable for the present application, in the linear regime, no existing material exhibits a positive Poisson's ratio equal or close to one. Some microstructures, however, have been shown to exist to manifest higher magnitudes of such ratio. In this respect, experimental evidence of negative Poisson's ratio materials, also known as auxetic materials, was reported by Lakes in 1987 [19]. In simple terms, one can recognize an auxetic material if any of its samples expands in the transverse direction of an imposed longitudinal elongation. In [20] a few cases of samples made of quasi-periodically porous materials undergoing moderate to large strains are examined. As it has already remarked in the previous section, whenever the samples do not undergo infinitesimal strains, the Poisson's ratio depend on the local measure of (nonlinear) strain. From now on we will refer to this as 'geometric Poisson's ratio'.

In [20] it is shown that auxetic behavior in compression is exhibited in some cases. This turns out to be a result of an occurring material instability. In particular, in [20] it is observed that a 2D periodic arrangement of circular voids, with an appropriate porous fraction, buckles under uniaxial compression, leading to a pattern of alternate mutually orthogonal ellipses. It is also demonstrated that high magnitudes of Poisson's ratio, sometimes close to -1, can be achieved by an appropriate selection of microstructure and void fraction. This suggests that a high magnitude of geometric Poisson's ratio could be in principle achieved in the case of inverse photonic crystals.

In this manuscript, we examine the photomechanical behaviour of two linear elastic PDMS matrices, each of which populated by a periodic distribution of cylindrical voids. The first case, shown in Figure 4a, has cylindrical voids in arranged in a square array (SA) configuration with a porosity f = 0.44. This basically reproduces what it is reported in [21]. The second situation, shown in Figure 4c, has a hexagonal array (HA) arrangement of voids and a porosity of f = 0.85. The interplanar spacing is d_0=240 nm for the SA and d_0=280 nm for the HA, chosen in order to achieve an identical initial bandgap wavelength of λ=600 nm.

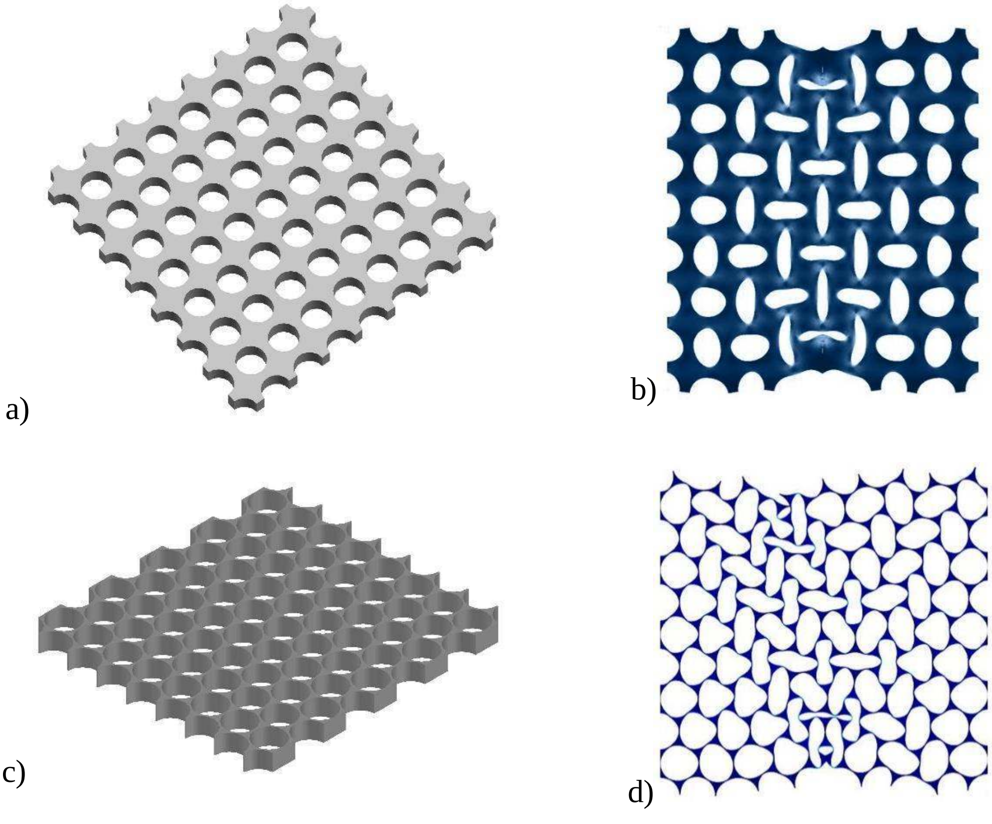

Figure 4. Square Array (SA) Hexagonal Array (HA) inverse crystals: initial (a,c) and deformed (b,d) configurations under imposed uniaxial contraction of ε_1=0.163.

The Finite Element Method (FEM) has been used to perform numerical simulations characterizing the mechanical behaviour of the inverse crystal under imposed contraction. The (virtually infinitely) long film is bonded onto the substrate (see fig. 3 b). Because of the fact that the horizontal displacement is transmitted through the boundary of the device, essentially at the edges of the sample, the elasticity of its support actually damps the effects of the loading. The damping distance scales with the following law: $h(E/E_s)^{1/3}$, where h is the deformed value of the thickness of the sensor and E, E_s are the apparent Young moduli of the crystal and substrate, respectively. The quantities E_s and h depend on the filling factor, which is strongly influenced by the large strains experienced by the polymer. For this reason, it is justified to examine the portion of the device directly influenced by the loading, although this is initially unknown. A nominal square domain is therefore chosen to illustrate the main features of the mechanical behaviour of the sensor. For the sake of simplicity, given that the expected regime is of moderately large strain(hence nonlinear) a quasi-incompressible Neo Hookean nonlinear elastic stress-strain law is assumed for both polymers.

COMSOL Multiphysics™ v5.0 has been used for the simulation. Standard solid prismatic isoparametric finite elements with triangular bases have been used for the discretization. The results of the analyses are illustrated in Figure 5. Figure 5a shows how Poisson's ratio ν changes with the compressive uniaxial strain ε_1. In both cases, ν is initially positive. Upon reaching a critical elongation value (ε_1=0.09 for SA and ε_1=0.14 for HA), the crystal starts buckling, producing distortion of the cylindrical voids.

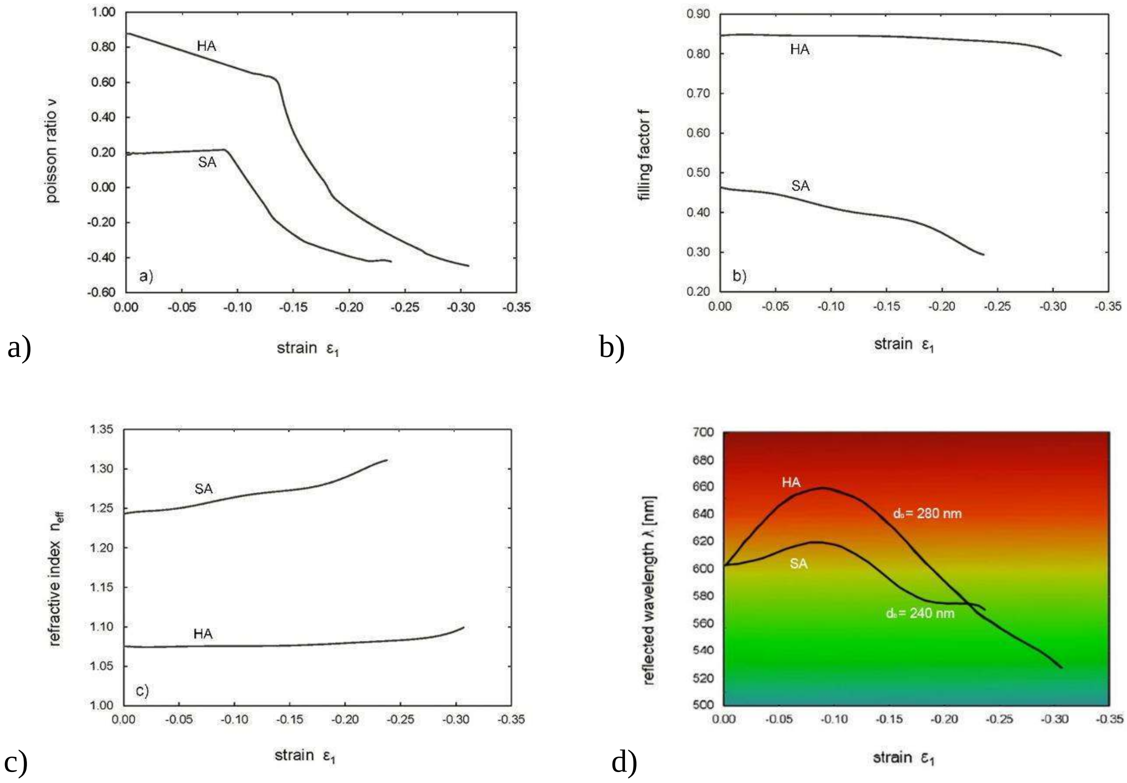

Figure 5. Results of the FEM simulations for a square array (SA) and a hexagonal array (HA) of voids: (a) geometric Poisson's ratio; (b) porosity; (c) effective refractive index; (d) reflected bandgap wavelength; all plotted against compressive strain.

The characteristic buckling patterns for the two configurations are shown in Figures 4b and 4d for a uniaxial contraction level of ε_1=0.163. Negative value of Poisson's ratio start occurring at local contraction values of ε_1=0.12 and ε_1=0.18 for the SA and HA configurations, respectively.

The reflected bandgap wavelength can be estimated, making use of a simplified expression as in Equation (7), where both refractive index and Poisson's coefficient change with the local strain induced by a corresponding compressive stress. A change in the effective refractive index is then expected as a result of the reduction in porosity caused by compression and buckling of the crystal. Figure 5b illustrates that the filling factor f changes with the amount of squeezing strain for both of the two crystal configurations. The effect of porosity, namely 1- f, on the refractive index is simulated through Equation (2) by assuming n_1 = 1.41 and n_2=1 for PDMS and air, respectively. The change in bandgap wavelength is eventually calculated and plotted in Figure 5d.

9. CONCLUSIONS

In this contribution we discussed the possibility of using mechano-photonic crystals as strain sensors. We first recall the feasibility of direct mechano-photonic structures obtained by using sub-micrometric polystyrene colloidal spheres in a PDMS matrix on a rubber substrate. For the direct structure specimens produced so far, the strain resolution is of the order of 350 με. This is insufficient for structural applications, where resolution of the order of few mε are typically required. The crystal sensitivity to strain depends directly on its interplanar spacing and on Poisson's ratio, which is most commonly limited to 0.3 for natural materials. We suggest to fabricate photonic crystal slabs to solve the challenge of realizing a cost-efficient and compact detection method, which could be useful for civil and mechanical engineering applications. We carried out a theoretical investigation to predict the opto-mechanical response of the PCSs.

REFERENCES

[1] L.P. Biró, J.P. Vigneron. Photonic nanoarchitectures in butterflies and beetles: valuable sources for bioinspiration. Laser Photonics Rev., **5**, 27-51, 2011.

[2] I. Bardyshev, A.D. Mokrushin, A.A. Pribylov, E.N. Samarov, V.M. Masalov, I.A. Karpov and G.A. Emelchenko, Porous structure of synthetic opals. Colloid J., 68, 20-25 (2006).

[3] J.M. Jethmalani, H.B. Sunkara, H.B. Ford, Optical diffraction from silica−poly (methyl methacrylate) composite films. Langmuir, **13**, 2633-2639, 1997.

[4] P. Jiang, J.F. Bertone, K.S. Hwang, V.L. Colvin, Single-Crystal colloidal multilayers of controlled thickness. Chem. Mater., **11**, 2132-2140, 1999.

[5] A. Chiappini, C. Armellini, A. Chiasera, M. Ferrari, Y. Jestin, M. Mattarelli, M. Montagna, E. Moser, G. Nunzi Conti, S. Pelli, G.C. Righini, M.C. Gonçalves, R.M. Almeida, Design of photonic structures by sol–gel-derived silica nanospheres, J. of Non-Cryst. Solids, **353**, 674-678, 2007.

[6] R.M. Measures, Structural monitoring with fiber optic technology. Academic Press (2001).

[7] B. Glisic, D. Inaudi, Fiber optic method for structural health monitoring. Wiley (2007).

[8] M. Pozzi, D. Zonta, H. Wu, D. Inaudi, Development and laboratory validation of in-line multiplexed low-coherence interferometric sensors. Optical Fiber Technology, **14**, 281–293, 2008.

[9] D. Zonta, B. Glisic, S. Adriaenssens, Value of information: impact of monitoring on decision-making. Structural Control and Health Monitoring, **21**, 1043–1056, 2014.

[10] C. Cappello, D. Zonta, M. Pozzi, R. Zandonini, Impact of prior perception on bridge health diagnosis. Journal of Civil Structural Health Monitoring, **5**, 509–525, 2015.

[11] C. Cappello, D. Zonta, B. Glisic, Expected utility theory for monitoring-based decision making. Proceedings of the IEEE. In press, 2016.

[12] H. Fudouzi, T. Sawada, Photonic rubber sheets with tunable color by elastic deformation. Langmuir, **22**, 1365-1368, 2006.

[13] H. Fudouzi, Soft opal films with tunable structural color and their applications. Proc. SPIE 6005, 22-30, 2005.

[14] D. Zonta, A. Chiappini, A. Chiasera, M. Ferrari, M. Pozzi, L. Battisti, M. Benedetti, Photonic crystals for monitoring fatigue phenomena in steel structures. Proc. SPIE 7292, 729215/1-10, 2008.

[15] Z.M. Wang, A. Neogi, Nanoscale Photonics and Optoelectronics. Springer, 65-69, 2010.

[16] R.M. Almeida, S. Portal, Photonic band gap structure by sol-gel processing. Curr. Opin. Solid St. M., **7**, 151-157, 2003.

[17] A. Chiappini, A. Piotrowska, M. Marciniak, M. Ferrari M. and D. Zonta, Design and fabrication of mechanochromic photonic crystals as strain sensor. Proc. SPIE. 9435, 94352M, 2015.

[18] E. Chow, S.Y. Lin, S.G. Johnson, P.R. Villeneuve, J.D. Joannopoulos, J.R. Wendt, G.A. Vawter, W. Zubrzycki, H. Hou, A. Alleman, Three-dimensional control of light in a two-dimensional photonic crystal slab, Nature, 407:983-986, 2000.

[19] S.R. Lakes, 1987, Foam structures with a negative Poisson's ratio. Science, 235:1038-1040, 1987.

[20] K. Bertoldi, P.M. Reis, S. Willshaw, T. Mullin, Negative Poisson's ratio behavior induced by an elastic instability. Adv. Mater., **22**, 361-366, 2010.

[21] J. T. B. Overvelde, S. Shan, and K. Bertoldi, Compaction Through Buckling in 2D Periodic, Soft and Porous Structures: Effect of Pore Shape. Adv. Mater., **24**, 2337-2342, 2012.